JACS
JOURNAL OF THE AMERICAN CHEMICAL SOCIETY
Article
pubs.acs.org/JACS

Modulation of Electronics and Thermal Stabilities of Photochromic Phosphino–Aminoazobenzene Derivatives in Weak-Link Approach Coordination Complexes

Jung Su Park,[†,§,∥] Alejo M. Lifschitz,[†,§] Ryan M. Young,[†,‡] Jose Mendez-Arroyo,[†] Michael R. Wasielewski,[†,‡] Charlotte L. Stern,[†,‡] and Chad A. Mirkin*[,†]

[†]Department of Chemistry and International Institute for Nanotechnology, Northwestern University, 2145 Sheridan Road, Evanston, Illinois 60208, United States

[‡]Argonne-Northwestern Solar Energy Research (ANSER) Center, Northwestern University, Evanston, Illinois 60208, United States

Supporting Information

ABSTRACT: A series of d^8 transition-metal (Pt(II) and Pd(II)) coordination complexes incorporating phosphine-functionalized aminoazobenzene derivatives as hemilabile phosphino–amine (P,N) ligands were synthesized and studied as model weak-link approach (WLA) photoresponsive constructs. The optical and photochemical properties of these complexes were found to be highly influenced by various tunable parameters in WLA systems, which include type of metal, coordination mode, type of ancillary ligand, solvent, and outer-sphere counteranions. In dichloromethane, reversible chelation and partial displacement of the P,N coordinating moieties allow for toggling between aminoazobenzene- or pseudostilbene- and azobenzene-type derivatives. The reversible switching between electronic states of azobenzene can be controlled through either addition or extraction of chloride counterions and is readily visualized in the separation between $\pi-\pi^*$ and $n-\pi^*$ bands in the complexes' electronic spectra. In acetonitrile solution, the WLA variables inherent to semiopen complexes have a significant impact on the half-lives of the corresponding *cis* isomers, allowing one to tune their half-lives from 20 to 21000 s, while maintaining photoisomerization behaviors with visible light. Therefore, one can significantly increase the thermal stability of a *cis*-aminoazobenzene derivative to the extent that single crystals for X-ray diffraction analysis can be grown for the first time, uncovering an unprecedented edge-to-face arrangement of the phenyl rings in the *cis* isomer. Overall, the azobenzene-functionalized model complexes shed light on the design parameters relevant for photocontrolled WLA molecular switches, as well as offer new ways of tuning the properties of azobenzene-based, photoresponsive materials.

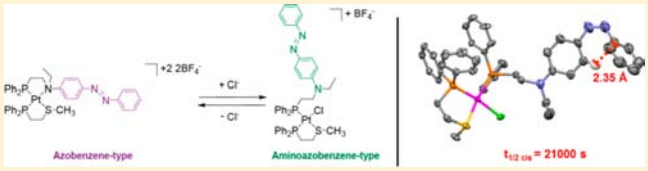

INTRODUCTION

Azobenzene and its analogues have long been scrutinized within the context of artificial photochromic systems capable of reversibly transforming between two isomeric forms possessing different electronic, structural, and functional properties.[1,2] This photoactive synthon has thus been exploited in photoresponsive molecular switches[3−6] in a variety of research areas ranging from industrial dyes[7,8] to actuators,[9] molecular machines,[10] liquid crystals,[11] nonlinear optical devices,[12] catalysts,[13] and biological applications.[14] These extensive studies have led to the general categorization of azobenzene derivatives into three types, namely azobenzene (AB), aminoazobenzene (aAB), and pseudostilbene types (pAB), on the basis of the relative energetic order of their $n-\pi^*$ and $\pi-\pi^*$ transition bands.[15,16] pAB- and aAB-type materials, obtained through attachments of electron-accepting and/or -donating moieties to the parent AB, display the desired red-shifted photoexcitation energies for isomerization in comparison to AB-type materials. However, both aAB and pAB exhibit significantly increased rates of thermal *cis* to *trans* isomerization, which may limit their use in applications that require longer-lived *cis* isomers.[15,16] Even though the AB family as a whole offers a wide span of photoexcitation energies and *cis* thermal stabilities,[1−16] there is still a major challenge to developing new synthetic approaches that allow for forward- and back-isomerization of AB with visible light and thermal stabilities of the corresponding *cis* isomers within a wide range of time scales. Among several synthetic strategies employed to control the photochemical properties given above, azo-conjugated transition-metal complexes have been shown to provide new advanced molecular functions via combinations of the remarkable photoswitching properties of AB and the magnetic, electrochemical, or coordination properties of the transition-metal complexes.[17−19]

We are particularly interested in exploiting the photochemistry of AB moieties in the context of the weak-link approach (WLA), a coordination chemistry based method for the construction of allosterically controlled supramolecular complexes.[20−22] This approach allows for modulating the

Received: July 12, 2013
Published: November 5, 2013

structure and properties of functional moieties embedded into the supramolecular architecture via coordination chemistry at distal sites, and it has been extensively employed in catalytic switches,[23,24] chemical sensors,[25,26] and signal amplification applications.[27,28] We envisioned that AB could bestow WLA systems with multiple new functionalities, since its photoisomerization can allow for the toggling of properties intrinsic to the behavior of catalytic switches, such as reactive cavity sizes and substrate binding affinities.[29,30] Furthermore, we hypothesized that AB could provide signaling for coordination changes that directly relate to the activity of a WLA system through the modulation of AB's electronics upon changes in coordination to the structural regulatory centers.

Toward this end, we have synthesized a series of model WLA d^8 transition-metal complexes (**3**−**12**) that incorporate hemilabile phosphino−amine (P,N) ligands **1** and **2** modified with two representative AB-conjugated moieties (Scheme 1). In doing so, we have discovered that the WLA provides a promising new platform for tailoring AB's photochemical properties through changes in programmable WLA parameters such as type of metal, coordination mode, type of ancillary ligand, solvent, and outer-sphere counteranions. For instance, it was determined that the switching between coordination modes via abstraction or addition of chloride (closed **9**−**12** vs semiopen **3**−**8**) induces dramatic electronic changes in parent AB chromophores, resulting in the toggling between two distinct types of AB derivatives in dichloromethane solution (AB vs aAB or pAB). While this toggling can be used, expectedly, to modulate the excitation energies for forward- and back-isomerization, we also determined that the WLA platform enables photochemical properties that are unique to the supramolecular ensemble. Most remarkably, we are able to generate semiopen complexes that retain the ability to be photoisomerized with visible light characteristic of aAB, while also being able to modulate the half-lives of their *cis* conformers over a 3 order of magnitude range, reaching values typical of AB-type moieties. Such control over their half-lives allows one to significantly increase the lifetime of *cis* isomers of aAB derivatives to the extent that single crystals can be grown at ambient temperature and structural characterization in the solid state is, for the first time, possible. The model complexes studied herein thus represent general photoactive building blocks that can be incorporated into new WLA supramolecular switches with unparalleled photochemical properties.

Scheme 1. Modulation of Photoisomerization Excitation Energies and *cis* Thermal Stabilities of Model WLA Complexes[a]

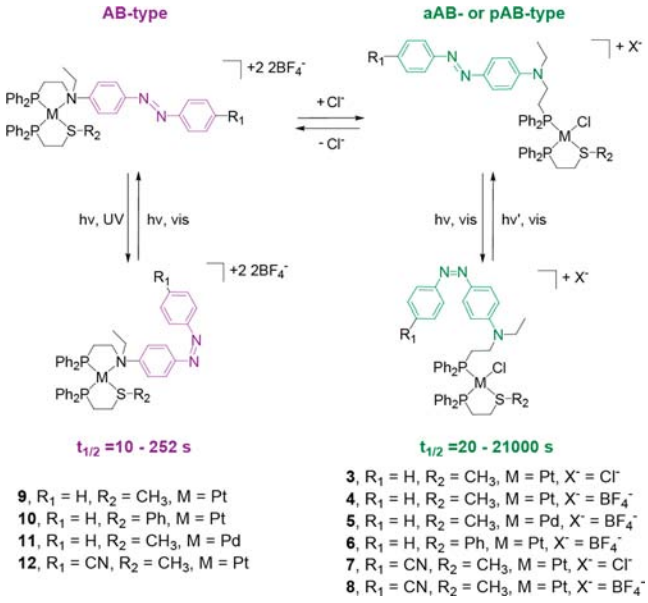

[a]The numbering of the compounds corresponds to the *trans* isomers unless otherwise noted.

RESULTS AND DISCUSSION

Synthesis. In many known cases, the azo group of AB can chelate to transition metals, thus hampering photoinduced *trans* to *cis* isomerization processes.[31] In order to avoid such a situation, it was hypothesized that the attachment of a phosphine moiety to aAB derivatives would not only result in P,N-based hemilabile ligands for WLA model complexes but could also prohibit the coordination of the azo group to soft WLA metal centers. Under this assumption, two photoisomerizable ligands possessing a P,N donor set, **1** and **2**, were prepared (see Scheme 2 and the Supporting Information). These azobenzene derivatives can be classified into aAB type for **1** and pAB type for **2** according to the Rau classification.[15,16]

Scheme 2. Synthetic Routes to Aminoazobenzene-Conjugated WLA Complexes

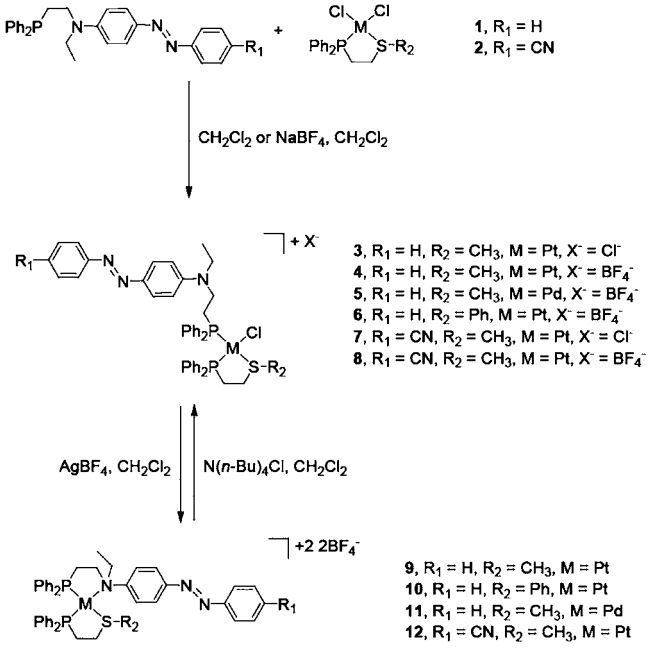

Using compounds **1** and **2**, a series of d^8 transition-metal complexes were successfully synthesized in high yields via well-established standard WLA protocols (Scheme 2).[32,33] The array of complexes as a whole introduces variables such as the nature of the metal cation (Pt(II) or Pd(II)), type of ancillary phosphino−thioether (P,S) ligand (P,S-Me or P,S-Ph) and inner- or outer-sphere anions (Cl^- and BF_4^-), which will be scrutinized later in terms of their effect on the photochemistry of the AB moieties. The model complexes were first isolated as semiopen complexes (**3**−**8**) in which the P,N-AB ligands are coordinated through the phosphorus to the transition-metal center and a second ancillary P,S ligand is chelated through

dx.doi.org/10.1021/ja407148n | J. Am. Chem. Soc. 2013, 135, 16988−16996

both phosphorus and sulfur moieties. The use of ancillary ligands illustrates the ability of the model complexes in question to be incorporated into larger functional systems, since these ligands have been shown to be easily replaced with isoelectronic moieties containing catalytic and substrate binding groups.[21,24] The semiopen complexes underwent quantitative chloride abstraction with $AgBF_4$ in CH_2Cl_2 to yield their closed counterparts (**9**–**12**) in which both the P,N-AB and ancillary ligands are chelated to the transition-metal center in a *cis* fashion. Reversible toggling between the closed and semiopen coordination modes is possible via the reintroduction of a chloride counterion in the form of $N(n\text{-}Bu)_4Cl$ (TBACl). A complete account of synthetic procedures and associated characterization data (^1H, $^{13}C\{^1H\}$, and $^{31}P\{^1H\}$ NMR and HRMS spectra) for compounds **1**–**12** is included in the Supporting Information.

Solid-State Characterization. To gain further insight into the details of structural parameters of AB-functionalized semiopen and closed complexes, X-ray crystallographic analyses of **1**, **3**–**5**, **7**, and **10** were carried out. As depicted in Figure 1,

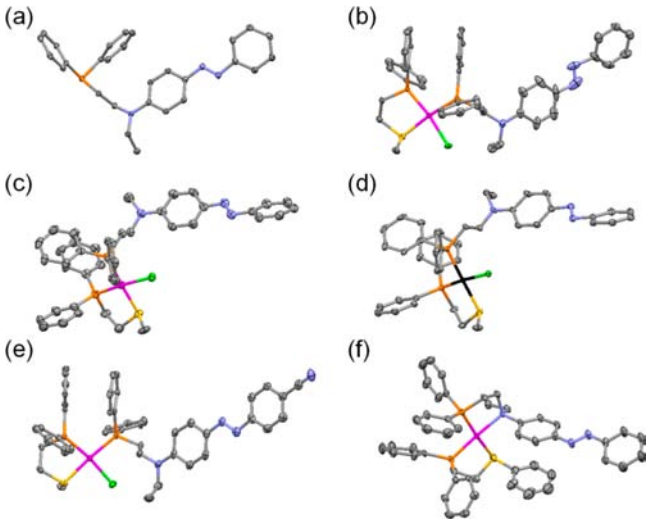

Figure 1. Crystal structures of **1** (a), **3** (b), **4** (c), **5** (d), **7** (e), and **10** (f) drawn with 50% probability thermal ellipsoids. Hydrogens and counteranions are omitted for clarity. Color scheme for the atoms: platinum, magenta; palladium, black; chloride, green; sulfur, yellow; phosphorus, orange; nitrogen, blue; carbon, gray.

these solid-state structural studies, in conjunction with solution-based characterization, serve to confirm our initial hypothesis that the novel aAB derivatives **1** and **2** would act as P,N-based hemilabile ligands which, significantly, do not undergo coordination of the azo groups to Pt(II) or Pd(II). A detailed inspection of these crystal structures reveals that the bond length parameters regarding the aAB moiety in semiopen complexes **3**–**5** are similar to those found in free ligand **1**. However, there is a significant difference in bond length parameters between the closed complex **10** and **1** or **3**–**5**. In particular, the distance of 1.48 Å between the nitrogen in the amino group and the 4-AB carbon in **10** is significantly longer than those found in either **1** or the semiopen complexes **3**–**5** (1.37 ± 0.01 Å). This can be rationalized upon consideration of the resonance structures of the aAB moiety. That is, the lone pair of electrons on the amino nitrogen engages in resonance structures that impart a partial double-bond character in ligand **1** and semiopen complexes **3**–**5** and, thus, contributes to the shortening of the N–C bond. Conversely, the nitrogen lone pair of electrons in **10** participates in the Pt–N coordination bond, which results in the lengthening of the N–C bond. Changes in the N–C bond length are highly indicative that metal coordination induces significant changes in the electronics of the aAB core.

Electronics and Photochemistry. UV–vis spectra of complexes **1**–**12** were measured in CH_2Cl_2 solutions in order to evaluate the effects of the metal cation and coordination mode on the electronic structures of the AB units. As exemplified in Figure 2, the electronic spectra of **1**–**8** display

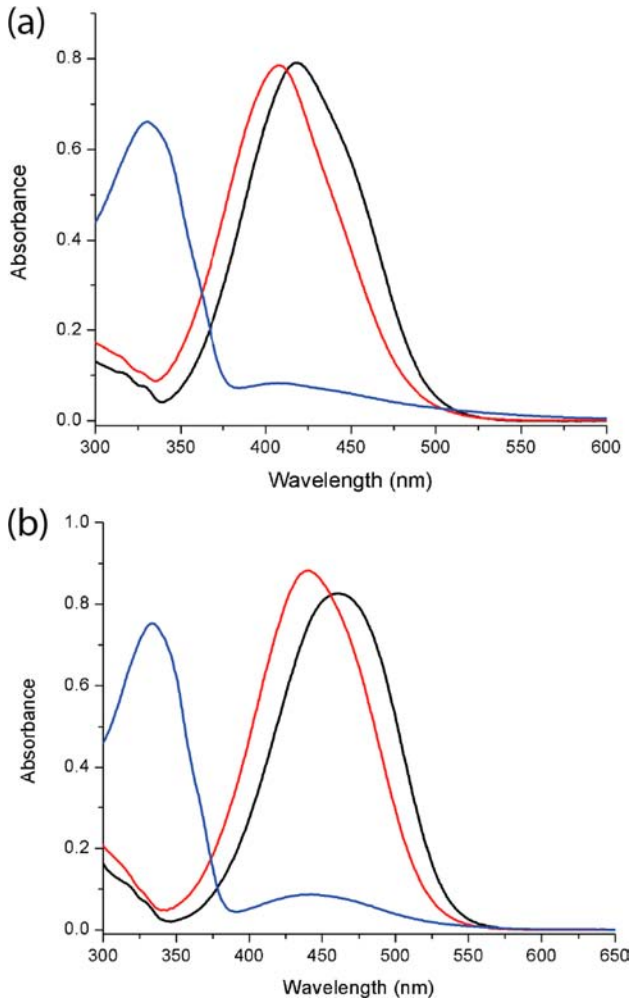

Figure 2. (a) Isomolar UV–vis spectra in CH_2Cl_2 of free ligand **1** (black), semiopen complex **4** (red), and closed complex **9** (blue). (b) Isomolar UV–vis spectra in CH_2Cl_2 of free ligand **2** (black), semiopen complex **8** (red), and closed complex **12** (blue).

a single broad absorption band in the visible region as a common feature. Only small blue shifts were observed in the λ_{max} values of semiopen complexes **3**–**8** as compared to those in the corresponding ligands **1** or **2** (see Table 1), suggesting that the formation of semiopen complexes does not alter the electronic structure of the aAB or pAB moieties significantly. Indeed, such large spectral overlap between π–π^* and n–π^* bands found in **1**–**8** is a key characteristic of either aAB- or pAB-type moieties. The electronic spectra of closed complexes **9**–**12**, however, are significantly different from those of **1**–**8** in terms of the separation between the π–π^* and n–π^* bands and

dx.doi.org/10.1021/ja407148n | J. Am. Chem. Soc. 2013, 135, 16988–16996

Table 1. λ_{max} Values of *trans* Forms of 1−12 Measured in CH_2Cl_2 and CH_3CN

compound	λ_{max} (nm) in CH_2Cl_2	λ_{max} (nm) in CH_3CN
1	418	418
2	461	459
3	410	411
4	408	411
5	408	411
6	408	411
7	444	445
8	446	445
9	330	409
10	331	409
11	321	407
12	334	440

their respective λ_{max} values (Figure 2). In particular, the UV−vis spectra of all closed complexes **9**−**12** display a high-intensity π−π^* band in the UV region which is well separated from a low-intensity n−π^* band in the visible region, overall a distinctive characteristic of AB-type materials.

As summarized in Table 1, the degree of blue shift in the absorption maxima of the closed complexes **9**−**12**, in comparison to **1** or **2**, depends on the type of metal cation and type of AB, regardless of solvent. For instance, chelation of the P,N group to Pd(II) induces a larger blue shift (**11**, $\Delta\lambda_{max}$ = 97 nm) than in Pt(II) complexes (**9**, $\Delta\lambda_{max}$ = 88 nm) for an identical ligand configuration. An even larger blue shift ($\Delta\lambda_{max}$ = 127 nm) was observed in the closed Pt(II) complex **12** from its parent pAB-type ligand **2**, in comparison to the **1** vs **9** pair (see Scheme 2). This latter finding can be rationalized from the cancellation of the push−pull character in **2** once the highly electron-donating ability of the amino group is diminished in **12** upon coordination to Pt(II).

Computational modeling further suggests that the spectral differences between semiopen and closed complexes result from the sequestration of the amino N lone pair of electrons upon coordination to a WLA metal center. Indeed, single-point calculations of semiopen complex **3** and closed complex **9** show that the azobenzene-centered orbitals involved in the transitions studied herein do not show an electronic contribution from the amino N lone pair in the closed Pt(II) complex **9** but do have a contribution in the azobenzene n and π^* orbitals of semiopen Pt(II) complex **3** (see the computational section in the Supporting Information).

The changes in electronic structures of AB chromophores induced by coordination of the P,N moieties result in dissimilar operation of the photoswitches between **1**−**8** and **9**−**12**. That is, closed complexes **9**−**12** undergo *trans* to *cis* isomerization upon irradiation at their λ_{max} values in the UV region and the corresponding back-isomerization process is achieved upon excitation of the n−π^* band in the visible region (410−550 nm). On the other hand, **1**−**8** undergo reversible photoisomerization triggered by irradiation at two visible light wavelengths, wherein forward-isomerization occurs upon irradiation at the λ_{max} of *trans* isomers **1**−**8** and back-isomerization occurs upon excitation at $\lambda \geq$525 nm for *cis*-**1** and *cis*-**3**−**6** or at $\lambda \geq$ 550 nm for *cis*-**2** and *cis*-**7**−**8**. The overall spectral changes described above indicate that the changes in coordination to Pt(II) or Pd(II) allow one to reversibly toggle between distinct electronic states of the azobenzene moieties by effectively varying the electron-donating ability of the nitrogen lone pair of electrons.

The toggling between electronic states of AB can also be exploited as a signaling tool for coordination changes. As mentioned above, the reversible switching between rigid, closed and flexible, open complexes by their interaction with appropriate allosteric effectors, a staple of the WLA, is also observed upon addition of a chloride ion source to closed complexes **9**−**12** in CH_2Cl_2. For instance, progressive additions of $N(n\text{-}Bu)_4Cl$ to complex **9** results in near-quantitative conversion to the corresponding semiopen complex **4**. $^{31}P\{^1H\}$ NMR spectra of the coordination complex mixture throughout the titration reveal that, indeed, each fraction of chloride added displaces the Pt−N bond selectively. This is supported by the decrease in the ^{31}P NMR signals corresponding to a closed heteroligated complex (δ 37.4, J_{P-P} = 14 Hz, J_{P-Pt} = 3298 Hz and δ 30.4, J_{P-P} = 14 Hz, J_{P-Pt} = 3216 Hz) and the concomitant increase in signals corresponding to a semiopen heteroligated complex comprised of chelated P,S (δ 43.9, J_{P-P} = 14 Hz, J_{P-Pt} = 3523 Hz) and phosphorus-bound P,N (δ 6.3, J_{P-P} = 15 Hz, J_{P-Pt} = 3124 Hz) ligands.[34] The titration process was also visualized by following the progressive UV−vis spectral variations produced from the changes in electronic structure of the AB moieties. As shown in Figure 3a, the titration results in the formation of an isosbestic point at 362 nm, thus establishing the signature of a two-state equilibrium between closed complex **9** and semiopen complex **4**, consistent with the $^{31}P\{^1H\}$ NMR measurements. Furthermore, changes in the absorption intensity of the complex mixture as a function of the respective $N(n\text{-}Bu)_4Cl$ concentrations were used to construct a binding isotherm and calculate the association constant (K_a = 9.2 × 106 M^{-1}). The high affinity of closed complexes for chloride anions in tandem with the large spectral changes that result from toggling between closed and semiopen complexes makes the AB moieties an excellent signaling unit for coordination changes in WLA complexes.

In order to further investigate the effects of WLA variables on the photochemical properties of AB in polar coordinating solvents, the electronic spectra of **1**−**12** were also measured in CH_3CN solutions. As summarized in Table 1, the λ_{max} values of *trans* isomers for **1**−**8** in CH_3CN are somewhat similar to those measured in CH_2Cl_2 solutions; the absorption properties in CH_3CN of semiopen complexes **3**−**8** and their corresponding free ligands **1** or **2** were also very similar to one other, displaying slightly blue shifted absorption maxima ($\Delta\lambda_{max}$ = 7 nm for **3**−**6** and $\Delta\lambda_{max}$ = 14 nm for **7** and **8**). It should be noted, however, that the cleanly closed complexes **9**−**12** cannot be made in CH_3CN solution, due to CH_3CN displacing the weak Pt−N coordination bond. Indeed, dissolving closed Pt(II) complexes **9**, **10**, and **12** in CH_3CN results in severe broadening of their $^{31}P\{^1H\}$ NMR signals, which suggests a fast dynamic exchange between closed and semiopen complexes caused by coordination of the solvent. In the case of Pd(II) complex **11**, however, two clean $^{31}P\{^1H\}$ NMR signals were observed (δ 64.0, J_{P-P} = 8 Hz and δ 29.2, J_{P-P} = 8 Hz), assigned to the CH_3CN-coordinated semiopen complex (**11b**). In all cases, coordination of CH_3CN is also supported by high-resolution mass spectroscopy measurements. The displacement of the coordinated amino group by CH_3CN is likely responsible for the significant red shifts observed in their λ_{max} values of **9**−**12**.

dx.doi.org/10.1021/ja407148n | J. Am. Chem. Soc. 2013, 135, 16988−16996

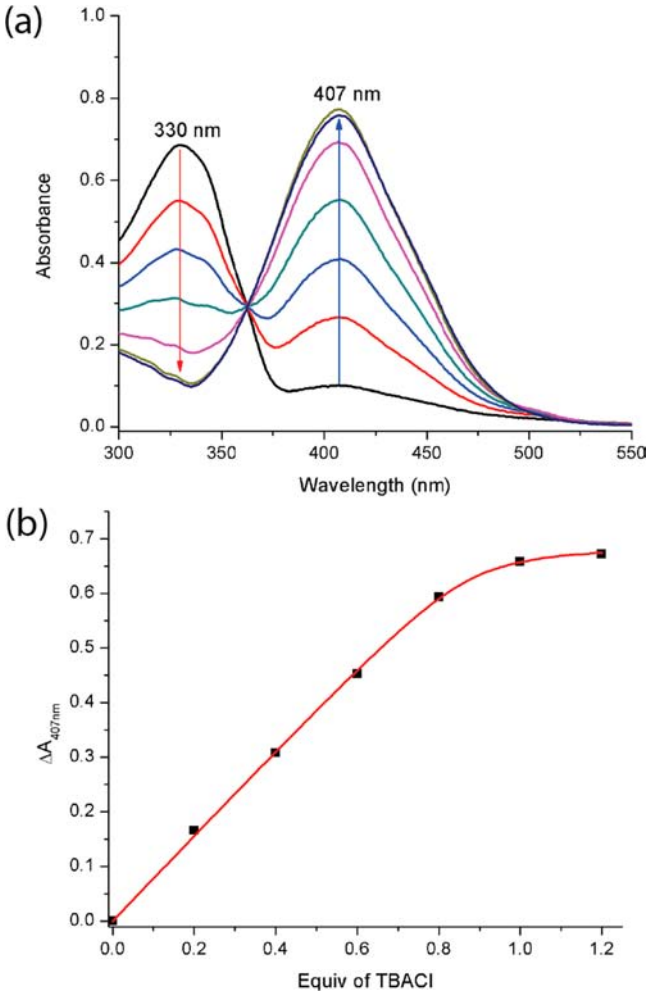

Figure 3. (a) Plot of UV−vis spectral changes of a 25 μM solution of closed complex **9** in CH_2Cl_2 arising as a function of increasing amounts of N(*n*-Bu)$_4$Cl and concomitant formation of semiopen complex **4**. (b) Binding curve analysis of chloride to complex **9** based on data in Figure 3a.

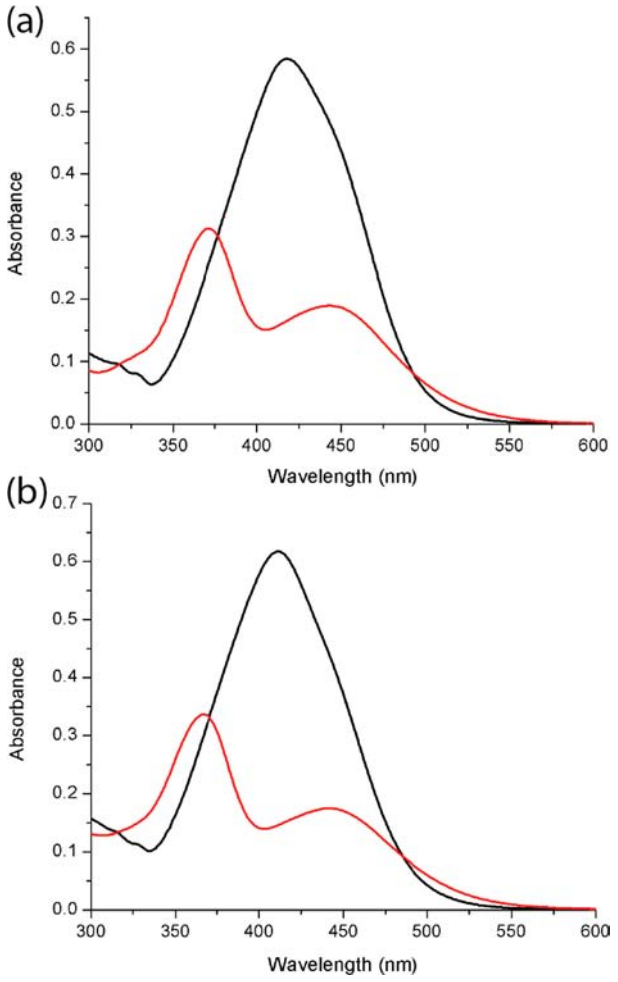

Figure 4. UV−vis spectral changes upon photoisomerization of **1** (a) and **4** (b) in CH_3CN before (black line) and after (red line) photoirradiation at the λ_{max} value of the corresponding *trans* isomer.

Upon irradiation at each complex's λ_{max}, all semiopen complexes undergo *trans* to *cis* photoisomerization. These photochromic effects are best exemplified by the corresponding changes in the measured UV−vis spectra of semiopen complexes **3**−**6** and **11** in CH_3CN; as shown in Figure 4b, the spectrum of *cis*-**4** in CH_3CN exhibits two distinct absorption bands centered at 367 and 441 nm following irradiation at λ_{ex} 418 nm, which are assigned to high-intensity $\pi-\pi^*$ and low-intensity n$-\pi^*$ excitation bands with the characteristic separation of the *cis*-aAB isomers. Similar changes in UV−vis spectra upon isomerization of free ligand **1** in CH_3CN and other corresponding semiopen complexes *cis*-**3**−**6** and *cis*-**11** were also obtained (see Figure 4a and the Supporting Information).

Thermal *cis* to *trans* Isomerization. As mentioned above, the thermal stability of *cis* conformers toward thermal isomerization is strongly influenced by the electronic structure of the AB derivative. In order to investigate the effects different WLA variables have on the stabilities of the *cis* isomers of **1**−**12**, rates of the thermal *cis* to *trans* isomerization were monitored in both CH_2Cl_2 and CH_3CN via UV−vis spectroscopy. Plots of the associated changes in absorption intensity as a function of time were then used to estimate first-order rate constants by nonlinear least-squares curve fit analyses, and the resulting values are summarized in Table 2.

In CH_2Cl_2 solution, improved *cis* thermal stabilities for both semiopen complexes *cis*-**3**−**8** and closed complexes *cis*-**9**−**12** were observed in general, in comparison to their free ligand counterparts, *cis*-**1** or *cis*-**2**; for a given combination of Pt(II) and the corresponding free ligands, the sequence closed > semiopen > free ligand was observed in terms of thermal stability of their *cis* isomers. We rationalize this order, in part, on the basis of considering that the closed Pt(II) complexes **9** and **10** behave as AB-type materials, which display greater *cis* half-lives than aAB-type materials across the board. As expected from the cancellation of push−pull character in the closed complex **12**, an even greater degree of stability of its *cis* isomer was observed in comparison to that of ligand **2**. Finally, it is worth noting that the stability of the *cis* conformers is higher in Pt(II) complexes than in Pd(II) complexes, given an identical set of ligands and coordination modes (*cis*-**4** *vs* *cis*-**5** and *cis*-**9** *vs* *cis*-**11**).

Significant solvent effects were also observed on the rates of thermal *cis* to *trans* isomerization of model WLA complexes. Most remarkably, it was found that rates of thermal *cis* to *trans* relaxation in acetonitrile are strongly influenced by variables associated with semiopen complexes such as type of metal, ancillary ligands, and outer-sphere counteranions. For instance,

dx.doi.org/10.1021/ja407148n | J. Am. Chem. Soc. 2013, 135, 16988−16996

Table 2. Rate Constants[a] of *cis* to *trans* Thermal Isomerization in CH_2Cl_2 and CH_3CN

	k/s^{-1} (half-life/s)	
compound	in CH_2Cl_2	in CH_3CN
cis-**1**	8.1×10^{-2} (8.5)	9.2×10^{-4} (750)
cis-**2**	9.6×10^{-2} (7.2)	1.4×10^{-2} (50)
cis-**3**	1.3×10^{-2} (54)	5.4×10^{-5} (13000)
cis-**4**	1.8×10^{-2} (39)	3.3×10^{-5} (21000)
cis-**5**	6.0×10^{-2} (12)	7.6×10^{-5} (9100)
cis-**6**	7.7×10^{-2} (9.1)	8.1×10^{-5} (8500)
cis-**7**	2.3×10^{-2} (30)	2.1×10^{-3} (330)
cis-**8**	2.1×10^{-2} (33)	2.1×10^{-3} (330)
cis-**9**	6.9×10^{-3} (100)	7.4×10^{-3} (94)[b]
cis-**10**	7.3×10^{-3} (95)	1.2×10^{-3} (56)[b]
cis-**11**/ *cis*-**11b**	6.7×10^{-2} (10)	3.4×10^{-2} (20)[c]
cis-**12**	2.8×10^{-3} (252)	1.6×10^{-2} (44)[b]

[a]All *k* values were calculated from the first-order plots of absorption change at 300 K in CH_2Cl_2 and CH_3CN. [b]The structure of the complex is part of a fast dynamic interchange between closed and semiopen coordination modes. [c]CH_3CN-coordinated semiopen complex.

complexes *cis*-**3**–**8**, having a coordinated chloride anion and semiopen configuration, generally have significantly longer half-lives than *cis*-**1** or *cis*-**2**. Furthermore, with a particular ligand combination, the stability of the *cis* conformers of Pt(II) complexes is higher than that for the Pd(II) counterparts (*cis*-**3** *vs* *cis*-**5**). The systems containing P,S-Me as an ancillary ligand show an enhanced thermal stability relative to those having P,S-Ph (*cis*-**4** *vs* *cis*-**6**). In addition, the complexes with BF_4^- as an outer-sphere counterion display *cis* stability higher than those with chloride. Finally, when a coordinated amine group in complexes **9**–**12** is replaced by CH_3CN, leading to the corresponding semiopen complexes, markedly decreased *cis* thermal stabilities are observed. These observations suggest that the overall WLA architecture, including the counterions and solvent molecules loosely associated with it, may affect the energetics and/or mechanism of the rearrangements undergone throughout thermal back-isomerization, effectively enabling a wide range of thermal stabilities of the *cis* conformer especially in polar coordinating solvents. Most notably, we can utilize the WLA architecture to access long-lived *cis* isomers of aAB-type materials while maintaining photoisomerization with visible light.

Crystal Structure of the Stabilized *cis*-aAB 4. To the best of our knowledge, there have been no reports of X-ray crystal structures of *cis*-aAB or *cis*-pAB-type molecules, although there are simulated molecular structures in the literature.[35−37] This is likely because of the fast thermal back-isomerization to the corresponding *trans* states, which makes it difficult to grow single crystals by conventional crystallization methods. The WLA platform, however, allows one to increase the thermal stability of *cis*-aAB moieties to the extent that, for the first time, crystallization is possible. Judging from thermal back-isomerization rates of *cis*-**1**–**8** in acetonitrile, complex *cis*-**4** possesses the highest thermal stability of the *cis* isomers across the board. We therefore attempted to grow diffraction-quality crystals of *cis*-**4** from an acetonitrile solution into which ether vapor was allowed to diffuse slowly after illumination with 411 nm band-filtered light. The resulting analysis of the crystals formed via this approach (Figure 5) reveals that the molecular structure of *cis*-**4** is significantly different from those of reported or

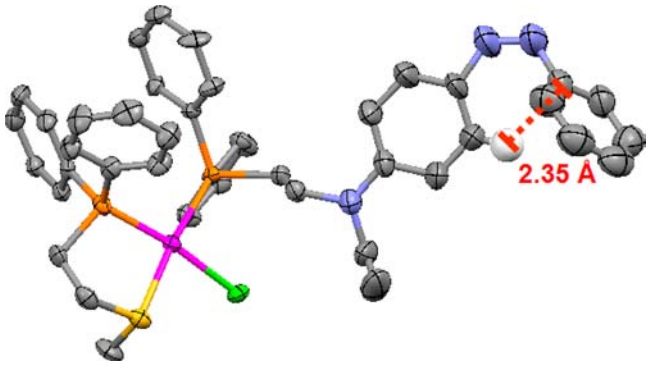

Figure 5. Crystal structure of *cis*-**4** drawn with 50% probability thermal ellipsoids. The hydrogen atom in close contact with one of the phenyl rings in the aAB moiety is shown. All other hydrogens and the counteranion are omitted for clarity. Color scheme for the atoms: platinum, magenta; chloride, green; sulfur, yellow; phosphorus, orange; nitrogen, blue; carbon, gray; hydrogen, white.

calculated *cis* isomers of AB and its analogues.[38−40] In particular, unlike the tilted face-to-face orientation of two phenyl rings found in all other reported *cis* structures, *cis*-**4** adopts an edge-to-face (T-shaped) structure. The significantly short distance between a β-positioned C−H moiety and a α-positioned carbon atom (2.35 Å) indicates an intermolecular CH−π interaction (H to ring plane distance of 2.38 Å). Although this kind of attractive intramolecular edge-to-face aromatic interaction is found in a variety of types of materials and plays an important role in such diverse areas as protein folding,[41,42] host−guest binding in supramolecular assemblies,[43] crystal packing and engineering,[44] drug−receptor interactions, and other molecular recognition processes,[45] this is the first observation of an intramolecular edge-to-face aromatic interaction for azobenzene derivatives.

Rates of Forward *trans* to *cis* Photoisomerization. After establishing that various parameters in the WLA system significantly influence the thermal *cis* to *trans* isomerization process, we went on to evaluate their influence on *trans* to *cis* photoisomerization quantum yields. Toward this end, samples of **1**–**8** in CH_2Cl_2 and CH_3CN were irradiated with a 440 nm laser diode and *trans* to *cis* isomerization rate constants were calculated from the time-dependent UV−vis spectral changes (see the Experimental Section for a full description of the setup). The quantum yields (Φ) were obtained by comparison to methyl orange standard (Φ = 0.47 in acetone). As summarized in Table 3, the quantum yields of *trans* to *cis* isomerization for all semiopen complexes **3**–**8** in both CH_2Cl_2 and CH_3CN solution were found to be lower than those of the

Table 3. Quantum Yields of *trans* to *cis* Photosomerization in CH_2Cl_2 and CH_3CN

	$\Phi_{trans-cis}$	
compound	in CH_2Cl_2	in CH_3CN
1	0.36	0.44
2	0.97	0.28
3	0.23	0.26
4	0.20	0.25
5	0.16	0.08
6	0.18	0.21
7	0.20	0.20
8	0.17	0.20

dx.doi.org/10.1021/ja407148n | J. Am. Chem. Soc. 2013, 135, 16988−16996

corresponding ligands as a common feature. We postulate that the decreases in quantum yields of *trans* to *cis* isomerization for semiopen WLA complexes with respect to the corresponding photochromic ligands arise in part due to the increase in the rotor volume for the motion of isomerization. It is worth noting, however, that the differences in quantum yields of photoinduced *trans* to *cis* isomerization between the semiopen complexes and their respective free ligands are far less than those observed for thermal *cis* to *trans* isomerization. Thus, the results described above indicate that changes in parameters in the WLA system can be used to modulate thermal stabilities of the *cis*-AB moieties, while roughly maintaining their *trans* to *cis* photoisomerization efficiency. Overall, the model complexes studied herein highlight the design considerations to be taken in the future construction of photoresponsive supramolecular devices via the WLA.

CONCLUSION

In summary, we have shown that the WLA architecture can be exploited to modulate the electronics and photophysical properties of AB moieties though various tunable WLA variables (type of metal cation, coordination mode, ancillary ligand, counteranions, and solvent). Coordination chemistry can be used to toggle between different types of AB, resulting in large changes in spectral features and photochromic behavior, which makes P,N-AB ligands potential signaling units for WLA sensors and signal amplification systems. Furthermore, the fact that WLA architecture and the counterions and solvent molecules loosely associated with it can impart aAB and pAB moieties with enhanced stabilities of their *cis* conformers suggests that thermally stable photoswitches operated solely with visible light can be generated by integrating different AB moieties into larger supramolecular systems. These photoactive moieties can thus be incorporated into WLA catalytic switches, and variables in the WLA system can then be defined so that the photoactive units exhibit the optimal *cis* state thermal stability for a particular reaction. Taken together, the findings in this study should pave the way to designing and synthesizing advanced photoswitchable supramolecular architectures with photoisomerization-dependent properties for catalysis and sensing applications.

EXPERIMENTAL SECTION

General Methods. P,N and P,S ligands were synthesized and stored using standard Schlenk line conditions, under an inert nitrogen atmosphere. The synthesis of semiopen and closed complexes was performed under ambient conditions. All solvents were purchased as HPLC grade and degassed under a stream of argon previous to use. Deuterated solvents were purchased from Cambridge Isotope Laboratories and used as received. All other chemicals were purchased from Aldrich Chemical Co. and used as received or synthesized according to literature procedures. NMR spectra were recorded on a Bruker Avance 400 MHz instrument. ^{1}H and ^{13}C{^{1}H} NMR spectra were referenced to residual proton and carbon resonances in the deuterated solvents. ^{31}P{^{1}H} NMR spectra were referenced to an 85% H_3PO_4 aqueous solution. All chemical shifts are reported in ppm. High-resolution electrospray ionization (ESI) mass spectra measurements were recorded on an Agilent 6120 LC-TOF instrument in positive ion mode. Electrospray ionization mass spectra (ESI-MS) were recorded on a Micromas Quatro II triple quadrapole mass spectrometer.

UV−vis absorption measurements were performed with a Varian Cary 50 Bio spectrophotometer utilizing 10 mm cell-path quartz cuvettes (VWR). Measurements of thermal *cis* to *trans* isomerization rates were performed using a 25 μM solution of **1**−**12**. A 3 mL portion of each sample was irradiated at the appropriate λ_{max} value in a Horiba Jovin-Yvonne Fluorolog fluorimeter with constant stirring and power outputs of ∼4 mW for 10 min. The samples were then placed in a UV−vis spectrophotometer, and their absorbance spectral changes were measured as a function of time at room temperature. Quantum yields of *trans* to *cis* photoisomerization were measured by exciting 2.50 mL samples of 25 μM solutions of **1**−**8** in CH_2Cl_2 or CH_3CN with a 440 nm laser diode (PicoQuant). Spectral changes in the solution upon excitation were monitored with a Shimadzu 1601 UV−vis spectrophotometer. The measurements were carried out with vigorous stirring and constant irradiation at 440 nm and power outputs of 0.85 mW. *trans* to *cis* isomerization rate constants were calculated from the time-dependent UV−vis spectral changes, and the values were used to calculate quantum yields of *trans* to *cis* photoisomerization as previously reported.[46] Methyl orange was used as a standard.[47,48]

Synthesis. *2-[N-[4-(Phenylazo)phenyl]-N-ethylamino]-1-methanesulfonate−Ethanol (**13**).* 2-[*N*-Ethyl-*N*-[4-[2-phenyldiazenyl]-phenyl]amino]ethanol[49] (8.00 g, 29.7 mmol) was dissolved in 100 mL of CH_2Cl_2 under an inert atmosphere, and triethylamine was added (20 mL). Methanesulfonyl chloride (10.2 g, 89.1 mmol, 3 equiv) in CH_2Cl_2 solution was slowly added, and the reaction mixture was stirred for 3 h. The solution was washed with water and dried over Na_2SO_4. The solvent was then evaporated, and the crude product was purified via silica gel column chromatography using CH_2Cl_2 as eluent, which afforded a dark red solid (9.91 g, 96% yield). ^{1}H NMR (400.16 MHz, 25 °C, CD_2Cl_2): δ 7.92 (d, J_{H-H} = 9 Hz, 2H), 7.86 (d, J_{H-H} = 9 Hz, 2H), 7.50 (m, 2H), 7.41 (t, J_{H-H} = 7 Hz, 1H), 6.84 (d, J_{H-H} = 9 Hz, 2H), 4.40 (t, J_{H-H} = 6 Hz, 2H), 3.80 (t, J_{H-H} = 6 Hz, 2H), 3.56 (q, J_{H-H} = 7 Hz, 2H), 2.98 (s, 3H), 1.26 (t, J_{H-H} = 7 Hz, 3H). ^{13}C{^{1}H} NMR (100.63 MHz, 25 °C, CD_2Cl_2): δ 150.5 (s), 144.1 (s), 130.5 (s), 130.1 (s), 129.4 (s), 126.0 (s), 122.5 (s), 112.3 (s), 67.0 (s), 49.9 (s), 46.5 (s), 37.9 (s), 12.4 (s). MS (ESI+): *m*/*z* calcd for $[M + H]^+$ 348, found 348.

*2-[N-[4-(4-Cyanophenylazo)phenyl]-N-ethylamino]-1-methanesulfonate−Ethanol (**14**).* The compound was prepared from 4-[2-[4-[ethyl(2-hydroxyethyl)amino]phenyl]diazenyl]benzonitrile[49] (9.00 g, 30.6 mmol) following the same mechanism as outlined above for **14**, which afforded an orange solid (10.8 g, 95% yield). ^{1}H NMR (400.16 MHz, 25 °C, CD_2Cl_2): δ 7.94 (m, 4H), 7.77 (d, J_{H-H} = 8 Hz, 2H), 6.84 (d, J_{H-H} = 9 Hz, 2H), 4.40 (t, J_{H-H} = 6 Hz, 2H), 3.82 (t, J_{H-H} = 6 Hz, 2H), 3.57 (q, J_{H-H} = 7 Hz, 2H), 2.98 (s, 3H), 1.27 (t, J_{H-H} = 7 Hz, 3H). ^{13}C{^{1}H} NMR (100.63 MHz, 25 °C, CD_2Cl_2): δ 192.2 (s), 151.6 (s), 144.2 (s), 134.4 (s), 133.6 (s), 126.8 (s), 123.0 (s), 119.2 (s), 112.33 (s), 66.8 (s), 49.9 (s), 46.6 (s), 37.9 (s), 12.4 (s). MS (ESI+): *m*/*z* calcd for $[M + H]^+$ 373, found 373.

*P,N-AB (**1**).* A sample of **13** (2.00 g, 5.76 mmol) was dissolved in 50 mL of tetrahydrofuran under an inert atmosphere, and the solution was cooled to 0 °C. A 0.5 M solution of $KPPh_2$ (11.5 mL, 1.00 equiv) was added in a dropwise fashion, and the mixture was stirred overnight at room temperature. The reaction was quenched by adding 10 mL of water, and the tetrahydrofuran was evaporated. The crude product was dissolved in CH_2Cl_2, and the solution was washed with water and dried over $MgSO_4$. Silica gel column chromatography using hexanes/CH_2Cl_2 (2/3, v/v) as eluent afforded the product as a dark red solid (0.504 g, 20% yield). ^{1}H NMR (400.16 MHz, 25 °C, CD_2Cl_2): δ 7.81 (d, J_{H-H} = 8 Hz, 2H), 7.77 (d, J_{H-H} = 9 Hz, 2H), 7.60−7.35 (m, 13H), 6.57 (d, J_{H-H} = 9 Hz, 2H), 3.49 (m, 2H), 3.43 (q, J_{H-H} = 7 Hz, 2H), 2.42 (m, 2H), 1.19 (t, J_{H-H} = 7 Hz, 3H). ^{13}C{^{1}H} NMR (100.63 MHz, 25 °C, CD_2Cl_2): δ 153.6 (s), 150.2 (s), 143.5 (s), 138.5 (d, J_{C-P} = 13 Hz), 133.2 (d, J_{C-P} = 19 Hz), 129.7 (s), 129.6 (s), 129.4 (s), 129.3 (s), 125.5 (s), 122.4 (s), 111.5 (s), 47.7 (d, J_{C-P} = 26 Hz), 45.6 (s), 26.6 (d, J_{C-P} = 15 Hz), 12.8 (s). ^{31}P{^{1}H} NMR (161.98 MHz, 25 °C, CD_2Cl_2): δ −20.8 (s). HRMS (ESI+): *m*/*z* calcd for $[M + H]^+$ 438.2021, found 438.2094.

*P,N-AB-CN (**2**).* The compound was prepared from **14** (2.00 g, 5.37 mmol) following the using the same procedure as outlined above for **1**. Silica-gel column chromatography using CH_2Cl_2 as eluent afforded the product as an orange solid (124 mg, 5% yield). ^{1}H NMR (400.16 MHz, 25 °C, CD_2Cl_2): δ 7.88 (d, J_{H-H} = 8 Hz, 2H), 7.79 (d, J_{H-H} = 8

dx.doi.org/10.1021/ja407148n | J. Am. Chem. Soc. 2013, 135, 16988−16996

Hz, 2H), 7.75 (d, J_{H-H} = 8 Hz, 2H), 7.60−7.35 (m, 10H), 6.55 (d, J_{H-H} = 8 Hz, 2H), 3.50 (m, 2H), 3.44 (q, J_{H-H} = 7 Hz, 2H), 2.42 (m, 2H), 1.19 (t, J_{H-H} = 7 Hz, 3H). $^{13}C\{^1H\}$ NMR (100.63 MHz, 25 °C, CD_2Cl_2): δ 155.8 (s), 151.1 (s), 143.6 (s), 138.3 (d, J_{C-P} = 13 Hz), 133.1 (d, J_{C-P} = 19 Hz), 129.4 (s), 129.1 (s), 129.0 (s), 122.9 (s), 119.3 (s), 112.2 (s), 111.6 (s), 47.8 (d, J_{C-P} = 26 Hz), 45.8 (s), 26.6 (d, J_{C-P} = 15 Hz), 12.7 (s). $^{31}P\{^1H\}$ NMR (161.98 MHz, 25 °C, CD_2Cl_2): δ −20.9 (s). HRMS (ESI+): *m/z* calcd for $[M + H]^+$ 463.2046, found 463.2046.

General Procedure for the Generation of Semiopen Complexes. Semiopen complexes were prepared as dichloride salts via dropwise addition of a solution of the ancilliary ligand (P,S-Me or P,S-Ph, 0.100 mmol) in 3 mL of CH_2Cl_2 to a suspension of dichloro(1,5-cyclooctadiene)platinum(II) (37.4 mg, 0.100 mmol) in 3 mL of CH_2Cl_2. After the mixture was stirred for 5 min, a solution of the corresponding AB-functionalized ligand (**1** or **2**, 0.100 mmol) in 3 mL of CH_2Cl_2 was added in a dropwise fashion. The solution volume was reduced to approximately 1 mL, and the product was precipitated with pentane. The product was collected via vacuum filtration and washed with pentane to afford the semiopen complex (in situ $^{31}P\{^1H\}$ NMR yields were quantitative, isolated yields were >95%). Semiopen complexes containing both Cl^- and BF_4^- counterions were prepared by dissolving the corresponding semiopen dichloride complex in 3 mL of CH_3OH in the presence of $AgBF_4$ (1.0 equiv). The mixture was stirred in the dark for 4 h, followed by solvent evaporation and dissolution in CH_2Cl_2. The mixture was filtered through a pad of Celite and recrystallized from a CH_2Cl_2/pentane mixture to afford the corresponding semiopen complex (in situ $^{31}P\{^1H\}$ NMR yields were quantitative, isolated yields were >95%).

[PtCl(κ$_2$-P,S-Me)(P,N-AB)]Cl ***(3)***. ^1H NMR (400.16 MHz, 25 °C, CD_2Cl_2): δ 8.00−7.05 (m, 27H), 6.47 (m, 2H), 4.05−2.40 (m, 12H), 1.82, (m, 1H) 1.16 (m, 3H). $^{31}P\{^1H\}$ NMR (161.98 MHz, 25 °C, CD_2Cl_2): δ 43.9 (d, J_{P-P} = 13 Hz, J_{P-Pt} = 3523 Hz, 1P), 6.3 (d, J_{P-P} = 14 Hz, J_{P-Pt} = 3123 Hz, 1P). HRMS (ESI+): *m/z* calcd for $[M - Cl]^+$ 928.2146, found 928.2155.

[PtCl(κ$_2$-P,S-Me)(P,N-AB)]BF$_4$ ***(4)***. ^1H NMR (400.16 MHz, 25 °C, CD_2Cl_2): δ 7.95−7.15 (m, 27H), 6.52 (m, 2H), 3.85−2.45 (m, 13H), 1.13 (t, J_{H-H} = 7 Hz, 3H). $^{31}P\{^1H\}$ NMR (161.98 MHz, 25 °C, CD_2Cl_2): δ 43.5 (d, J_{P-P} = 13 Hz, J_{P-Pt} = 3510 Hz, 1P), 6.2 (d, J_{P-P} = 14 Hz, J_{P-Pt} = 3155 Hz, 1P). HRMS (ESI+): *m/z* calcd for $[M - Cl]^+$ 928.2146, found 928.2148.

[PdCl(κ$_2$-P,S-Me)(P,N-AB)]BF$_4$ ***(5)***. ^1H NMR (400.16 MHz, 25 °C, CD_2Cl_2): δ 7.81 (d, J_{H-H} = 8 Hz, 2H), 7.74 (d, J_{H-H} = 8 Hz, 2H), 7.59−7.35 (m, 23H), 6.49 (m, 2H), 3.65 (s, 2H), 3.37 (m, 2H), 3.18 (s, 2H), 2.95 (s, 3H), 2.80 (m, 2H), 2.63 (m, 2H), 1.14 (t, J_{H-H} = 7 Hz, 3H). $^{31}P\{^1H\}$ NMR (161.98 MHz, 25 °C, CD_2Cl_2): δ 62.9 (d, J_{P-P} = 5 Hz, 1P), 20.6 (d, J_{P-P} = 5 Hz, 1P). HRMS (ESI+): *m/z* calcd for $[M - Cl]^+$ 840.1533, found 840.1544.

[PtCl(κ$_2$-P,S-Ph)(P,N-AB)]BF$_4$ ***(6)***. ^1H NMR (400.16 MHz, 25 °C, CD_2Cl_2): δ 8.20−7.10 (m, 32H), 6.50 (m, 2H), 3.87−2.55 (m, 9H), 1.75−0.85 (m, 4H). $^{31}P\{^1H\}$ NMR (161.98 MHz, 25 °C, CD_2Cl_2): δ 44.2 (d, J_{P-P} = 15 Hz, J_{P-Pt} = 3497 Hz, 1P), 6.3 (d, J_{P-P} = 15 Hz, J_{P-Pt} = 3201 Hz, 1P). HRMS (ESI+): *m/z* calcd for $[M - Cl]^+$ 990.2304, found 990.2310.

[PtCl(κ$_2$-P,S-Me)(P,N-AB-CN)]Cl ***(7)***. ^1H NMR (400.16 MHz, 25 °C, CD_2Cl_2): δ 8.05−6.40 (m, 28H), 4.25−1.05 (m, 16H). $^{31}P\{^1H\}$ NMR (161.98 MHz, 25 °C, CD_2Cl_2): δ 43.6 (d, J_{P-P} = 13 Hz, J_{P-Pt} = 3492 Hz, 1P), 6.0 (d, J_{P-P} = 13 Hz, J_{P-Pt} = 3121 Hz, 1P). HRMS (ESI+): *m/z* calcd for $[M - Cl]^+$ 953.2099, found 953.2097.

[PtCl(κ$_2$-P,S-Me)(P,N-AB-CN)]BF$_4$ ***(8)***. ^1H NMR (400.16 MHz, 25 °C, CD_2Cl_2): δ 7.88 (d, J_{H-H} = 8 Hz, 2H), 7.79−7.15 (m, 23H), 6.51 (m, 3H), 3.71 (m, 2H), 3.38 (m, 2H), 3.32−2.40 (m, 9H), 1.16 (t, J_{H-H} = 7 Hz, 3H). $^{31}P\{^1H\}$ NMR (161.98 MHz, 25 °C, CD_2Cl_2): δ 43.9 (d, J_{P-P} = 15 Hz, J_{P-Pt} = 3507 Hz, 1P), 6.3 (d, J_{P-P} = 15 Hz, J_{P-Pt} = 3125 Hz, 1P). HRMS (ESI+): *m/z* calcd for $[M - Cl]^+$ 953.2099, found 953.2109.

General Procedure for the Generation of Closed Complexes. A sample of semiopen complex containing one BF_4^- and one Cl^- counterion (0.100 mmol) was dissolved in 3 mL of CH_2Cl_2, and $AgBF_4$ (21.7 mg, 1.10 equiv, 0.110 mmol) was added. The mixture was stirred in the dark for 15 min. The mixture was then filtered through a pad of Celite, and the product was recrystallized from a CH_2Cl_2/pentane mixture to afford the corresponding closed complex (in situ $^{31}P\{^1H\}$ NMR yields were quantitative, isolated yields were >95%).

[Pt(κ$_2$-P,S-Me)(κ$_2$-P,N-AB)](BF$_4$)$_2$ ***(9)***. ^1H NMR (400.16 MHz, 25 °C, CD_2Cl_2): δ 8.13 (d, J_{H-H} = 7 Hz, 2H), 7.97 (d, J_{H-H} = 7 Hz, 2H), 7.85−7.35 (m, 24H), 4.51 (m, 2H), 4.00−1.02 (m, 14H). $^{31}P\{^1H\}$ NMR (161.98 MHz, 25 °C, CD_2Cl_2): δ 37.4 (d, J_{P-P} = 15 Hz, J_{P-Pt} = 3308 Hz, 1P), 30.4 (d, J_{P-P} = 15 Hz, J_{P-Pt} = 3215 Hz, 1P). HRMS (ESI+): *m/z* calcd for $[M - BF_4]^+$ 980.2488, found 980.2485.

[Pt(κ$_2$-P,S-Ph)(κ$_2$-P,N-AB)](BF$_4$)$_2$ ***(10)***. ^1H NMR (400.16 MHz, 25 °C, CD_2Cl_2): δ 820−6.55 (m, 34H), 4.40−0.90 (m, 13H). $^{31}P\{^1H\}$ NMR (161.98 MHz, 25 °C, CD_2Cl_2): δ 37.8 (d, J_{P-P} = 15 Hz, J_{P-Pt} = 3374 Hz, 1P), 30.9 (d, J_{P-P} = 15 Hz, J_{P-Pt} = 3188 Hz, 1P). HRMS (ESI+): *m/z* calcd for $[M - BF_4]^+$ 1041.2643, found 1041.2647.

[Pd(κ$_2$-P,S-Me)(κ$_2$-P,N-AB)](BF$_4$)$_2$ ***(11)***. ^1H NMR (400.16 MHz, 25 °C, CD_2Cl_2): δ 8.09 (d, J_{H-H} = 8 Hz, 2H), 7.95 (d, J_{H-H} = 7 Hz, 2H), 7.70−7.00 (m, 25H), 4.42 (s, 2H), 3.75−2.52 (m, 7H), 1.85 (s, 3H), 1.64 (s, 1H), 1.48 (t, J_{H-H} = 7 Hz, 3H). $^{31}P\{^1H\}$ NMR (161.98 MHz, 25 °C, CD_2Cl_2): δ 58.4 (d, J_{P-P} = 8 Hz, 1P), 53.6 (d, J_{P-P} = 6 Hz, 1P). HRMS (ESI+): *m/z* calcd for $[M - BF_4]^+$ 891.1907, found 891.1916.

[Pd(CH$_3$CN)(κ$_2$-P,S-Me)(P,N-AB)](BF$_4$)$_2$ ***(11b)***. ^1H NMR (400.16 MHz, 25 °C, CD_3CN): δ 7.88−7.30 (m, 27H), 6.77 (d, J_{H-H} = 8 Hz, 2H), 3.75−2.52 (m, 7H), 3.477−2.47 (m, 12H), 2.11 (s, 3H), 1.28−0.87 (m, 4H). $^{31}P\{^1H\}$ NMR (161.98 MHz, 25 °C, CD_3CN): δ 63.9 (d, J_{P-P} = 6 Hz, 1P), 29.2 (d, J_{P-P} = 6 Hz, 1P). HRMS (ESI+): *m/z* calcd for $[M - BF_4]^+$ 932.2172, found 932.2175.

[Pt(κ$_2$-P,S-Me)(κ$_2$-P,N-AB-CN)](BF$_4$)$_2$ ***(12)***. ^1H NMR (400.16 MHz, 25 °C, CD_2Cl_2): δ 8.18 (d, J_{H-H} = 8 Hz, 2H), 8.04 (d, J_{H-H} = 8 Hz, 2H), 7.85 (d, J_{H-H} = 8 Hz, 2H), 7.73−6.95 (m, 22H), 4.51 (m, 2H), 3.94−2.53 (m, 8H), 2.12−0.85 (m, 6H). $^{31}P\{^1H\}$ NMR (161.98 MHz, 25 °C, CD_2Cl_2): δ 37.3 (d, J_{P-P} = 14 Hz, J_{P-Pt} = 3324 Hz, 1P), 30.6 (d, J_{P-P} = 13 Hz, J_{P-Pt} = 3222 Hz, 1P). HRMS (ESI+): *m/z* calcd for $[M - BF_4]^+$ 1005.2440, found 1005.2449.

X-ray Crystallography. Crystallographic data are displayed in the Supporting Information (Table S1). Single crystals were mounted using oil (Infineum V8512) on a glass fiber. All measurements were made with a CCD area detector with graphite-monochromated Cu Kα radiation. Data were collected using a Bruker APEXII detector and processed using APEX2 from Bruker. All structures were solved by direct methods and expanded using Fourier techniques. The non-hydrogen atoms were refined anisotropically. Hydrogen atoms were included in idealized positions but not refined. Their positions were constrained relative to their parent atom using the appropriate HFIX command in SHELXL-97.

■ ASSOCIATED CONTENT

Ⓢ Supporting Information

Figures and tables giving UV−vis spectra of all species before and after irradiation at their respective photostations, absorbance vs time plots for thermal *cis* to *trans* isomerization and *trans* to *cis* photoisomerization, crystallographic data for **1**, **3**, **4**, *cis*-**4**, **5**, **7**, and **10**, and NMR spectra for **1**−**12**. This material is available free of charge via the Internet at http://pubs.acs.org.

■ AUTHOR INFORMATION

Corresponding Author

C.A.M.: e-mail, chadnano@northwestern.edu; fax, (1) 847-467-5123.

Present Address

[‖]Department of Chemistry, College of Science, Sookmyung Women's University, Cheongpa-dong 2-ga, Yonsan-gu, Seoul 140-742, Korea.

Author Contributions

[§]These authors contributed equally.

Notes

The authors declare no competing financial interest.

■ ACKNOWLEDGMENTS

This material is based upon work supported by DoD/NSSEFF/NPS awards N00244-09-1-0012 and N00244-09-1-0071, U.S. Army award W911NF-11-1-0229, NSF award CHE-1149314, and Basic Science Research Programs through the National Research Foundation of Korea (NRF) funded by the Ministry of Science, ICT and Future Planning (NRF-2013R1A1A1011508). M.R.W. was supported by the Chemical Sciences, Geosciences, and Biosciences Division, Office of Basic Energy Sciences, DOE, under Grant No. DE-FG02-99ER14999. R.M.Y. was supported as part of the ANSER Center, an Energy Frontier Research Center funded by the U.S. Department of Energy (DOE), Office of Science, Office of Basic Energy Sciences, under award number DE-SC0001059. R.M.Y. also thanks the Camille and Henry Dreyfus Postdoctoral Program in Environmental Chemistry for support.

■ REFERENCES

(1) Feringa, B. L. *Molecular Switches*; Wiley-VCH: Weinheim, Germany, 2001.
(2) Balzani, V.; Credi, A.; Venturi, M. *Nano Today* **2007**, *2*, 18.
(3) Yamada, M.; Kondo, M.; Mamiya, J.-i.; Yu, Y.; Kinoshita, M.; Barrett, Christopher, J.; Ikeda, T. *Angew. Chem., Int. Ed.* **2008**, *47*, 4986.
(4) Russew, M. M.; Hecht, S. *Adv. Mater.* **2010**, *22*, 3348.
(5) Puntoriero, F.; Ceroni, P.; Balzani, V.; Bergamini, G.; Vogtle, F. *J. Am. Chem. Soc.* **2007**, *129*, 10714.
(6) Parker, R. M.; Gates, J. C.; Rogers, H. L.; Smith, P. G. R.; Grossel, M. C. *J. Mater. Chem.* **2010**, *20*, 9118.
(7) Venkataraman, K. *The Chemistry of Synthetic Dyes*; Academic Press: New York, 1970; Vols. *1*−*7*.
(8) He, T. C., Y.; Du, Y.; Mo, Y. *Opt. Commun.* **2007**, *275*, 240.
(9) Bleger, D.; Yu, Z. L.; Hecht, S. *Chem. Commun.* **2011**, *47*, 12260.
(10) Kay, E. R.; Leigh, D. A.; Zerbetto, F. *Angew. Chem., Int. Ed.* **2007**, *46*, 72.
(11) Yu, H. F.; Ikeda, T. *Adv. Mater.* **2011**, *23*, 2149.
(12) Delaire, J. A.; Nakatani, K. *Chem. Rev.* **2000**, *100*, 1817.
(13) Stoll, R. S.; Hecht, S. *Angew. Chem., Int. Ed.* **2010**, *49*, 5054.
(14) Beharry, A. A.; Woolley, G. A. *Chem. Soc. Rev.* **2011**, *40*, 4422.
(15) Hamon, F.; Djedaini-Pilard, F.; Barbot, F.; Len, C. *Tetrahedron* **2009**, *65*, 10105.
(16) Bandara, H. M. D.; Burdette, S. C. *Chem. Soc. Rev.* **2012**, *41*, 1809.
(17) Dogan, A.; Sarkar, B.; Klein, A.; Lissner, F.; Schleid, T.; Fiedler, J.; Zalis, S.; Jain, V. K.; Kaim, W. *Inorg. Chem.* **2004**, *43*, 5973.
(18) Kume, S.; Nishihara, H. *Dalton Trans.* **2008**, 3260.
(19) Samanta, S.; Ghosh, P.; Goswami, S. *Dalton Trans.* **2012**, *41*, 2213.
(20) Wiester, M. J.; Ulmann, P. A.; Mirkin, C. A. *Angew. Chem., Int. Ed.* **2011**, *50*, 114.
(21) Gianneschi, N. C.; Masar, M. S.; Mirkin, C. A. *Acc. Chem. Res.* **2005**, *38*, 825.
(22) Holliday, B. J.; Mirkin, C. A. *Angew. Chem., Int. Ed.* **2001**, *40*, 2022.
(23) Oliveri, C. G.; Gianneschi, N. C.; Nguyen, S. T.; Mirkin, C. A.; Stern, C. L.; Wawrzak, Z.; Pink, M. *J. Am. Chem. Soc.* **2006**, *128*, 16286.
(24) Ulmann, P. A.; Braunschweig, A. B.; Lee, O. S.; Wiester, M. J.; Schatz, G. C.; Mirkin, C. A. *Chem. Commun.* **2009**, 5121.
(25) Jeon, Y. M.; Kim, D.; Mirkin, C. A.; Golen, J. A.; Rheingold, A. L. *Tetrahedron* **2008**, *64*, 8428.
(26) Lifschitz, A. M.; Shade, C. M.; Spokoyny, A. M.; Mendez-Arroyo, J.; Stern, C. L.; Sarjeant, A. A.; Mirkin, C. A. *Inorg. Chem.* **2013**, *52*, 5484.
(27) Masar, M. S.; Gianneschi, N. C.; Oliveri, C. G.; Stern, C. L.; Nguyen, S. T.; Mirkin, C. A. *J. Am. Chem. Soc.* **2007**, *129*, 10149.
(28) Yoon, H. J.; Kuwabara, J.; Kim, J. H.; Mirkin, C. A. *Science* **2010**, *330*, 66.
(29) Banghart, M.; Borges, K.; Isacoff, E.; Trauner, D.; Kramer, R. H. *Nat. Neurosci.* **2004**, *7*, 1381.
(30) Shimoboji, T.; Larenas, E.; Fowler, T.; Kulkarni, S.; Hoffman, A. S.; Stayton, P. S. *Proc. Natl. Acad. Sci. U.S.A.* **2002**, *99*, 16592.
(31) Zenkina, O.; Altman, M.; Leitus, G.; Shimon, L. J. W.; Cohen, R.; van der Boom, M. E. *Organometallics* **2007**, *26*, 4528.
(32) Ulmann, P. A.; Brown, A. M.; Ovchinnikov, M. V.; Mirkin, C. A.; DiPasquale, A. G.; Rheingold, A. L. *Chem. Eur. J.* **2007**, *13*, 4529.
(33) Ulmann, P. A.; Mirkin, C. A.; DiPasquale, A. G.; Liable-Sands, L. M.; Rheingold, A. L. *Organometallics* **2009**, *28*, 1068.
(34) Garrou, P. E. *Chem. Rev.* **1981**, *81*, 229.
(35) Bassotti, E.; Carbone, P.; Credi, A.; Di Stefano, M.; Masiero, S.; Negri, F.; Orlandi, G.; Spada, G. P. *J. Phys. Chem. A* **2006**, *110*, 12385.
(36) Wang, L. X.; Wang, X. G. *J. Mol. Struct. (THEOCHEM)* **2007**, *806*, 179.
(37) Dokic, J.; Gothe, M.; Wirth, J.; Peters, M. V.; Schwarz, J.; Hecht, S.; Saalfrank, P. *J. Phys. Chem. A* **2009**, *113*, 6763.
(38) Kurita, N.; Tanaka, S.; Itoh, S. *J. Phys. Chem. A* **2000**, *104*, 8114.
(39) Biswas, N.; Umapathy, S. *J. Phys. Chem. A* **1997**, *101*, 5555.
(40) Beveridg, Dl; Jaffe, H. H. *J. Am. Chem. Soc.* **1966**, *88*, 1948.
(41) Chakrabarti, P.; Samanta, U. *J. Mol. Biol.* **1995**, *251*, 9.
(42) Brandl, M.; Weiss, M. S.; Jabs, A.; Suhnel, J.; Hilgenfeld, R. *J. Mol. Biol.* **2001**, *307*, 357.
(43) Takahashi, H.; Tsuboyama, S.; Umezawa, Y.; Honda, K.; Nishio, M. *Tetrahedron* **2000**, *56*, 6185.
(44) Umezawa, Y.; Tsuboyama, S.; Honda, K.; Uzawa, J.; Nishio, M. *Bull. Chem. Soc. Jpn.* **1998**, *71*, 1207.
(45) Ramirez-Gualito, K.; Alonso-Rios, R.; Quiroz-Garcia, B.; Rojas-Aguilar, A.; Diaz, D.; Jimenez-Barbero, J.; Cuevas, G. *J. Am. Chem. Soc.* **2009**, *131*, 18129.
(46) Suwa, K.; Otsuki, J.; Goto, K. *J. Phys. Chem. A* **2010**, *114*, 884.
(47) Takei, M.; Yui, H.; Hirose, Y.; Sawada, T. *J. Phys. Chem. A* **2001**, *105*, 11395.
(48) Bandara, H. M. D.; Burdette, S. C. *Chem. Soc. Rev.* **2012**, *41*, 1809.
(49) Vijayakumar, C.; Balan, B.; Kim, M. J.; Takeuchi, M. *J. Phys. Chem. C* **2011**, *115*, 4533.